national accelerator laboratory

FN-278
1103.000
7700.108

ENERGY DEPOSITION IN THICK TARGETS BY HIGH ENERGY PROTONS: MEASUREMENT AND CALCULATION

September, 1975

M. Awschalom, P. J. Gollon, C. Moore, A. Van Ginneken

ABSTRACT

Calorimetric measurements of energy deposition by 300 GeV protons are reported in narrow Be, Al, Cu and W targets, several interaction lengths long. Monte Carlo predictions of the same quantities are also presented. The agreements between measurements and calculations are very good.

I. INTRODUCTION

Over the last decade, Monte Carlo techniques[1] have been used with increasing frequency and at higher energies, for the simulation of hadron transport, including the description of extra-nuclear hadron cascades. These techniques are used to make predictions concerning performance of high energy accelerator shielding, cosmic ray spectra, ionization calorimeters, and other phenomena involving interactions of many generations of particles in bulk matter. As part of a program to test the accuracy of, and provide benchmark data for extra-nuclear cascade calculations, we have measured the energy deposition (i.e., thermal heating) by 300 GeV protons in targets several interaction lengths long[2]. This provides information on the development of the core of the hadron cascade. This information is directly applicable to the design of collimators and targets for particle accelerators of the highest energies.

II. EXPERIMENTAL TECHNIQUE

A. Targets

Four elements were used as targets: Be, Al, Cu, and W. These permitted a wide range of atomic numbers to be studied, and provided large variations in the ratio of the nucleon non-elastic mean free path to the radiation length, see Table I.

Each target set consisted of six cylinders mounted coaxially with the incident proton beam. Proceeding in the beam direction, their lengths were approximately $\lambda/4$, $\lambda/2$, $\lambda/2$, λ, λ and λ; where λ is the interaction length (non-elastic mean free path).

The main series of measurements used a target diameter of 2.54 cm; this was a compromise between the advantage a narrow target gave in studying the central cascade region, and the lesser sensitivity of a larger diameter target to variations in beam size, position and alignment. Additional measurements were made with 5.08 cm diameter Al and Cu targets.

Each target set was mounted in a styrofoam calorimeter[3] which insulated each segment from the environment and from adjacent segments, Fig. 1. Target cylinders were separated by 3.76 cm of foam insulation. These target assemblies were placed on a movable table which was used to position them in the beam at the time of the irradiation.

Thermistors[4] were placed in close thermal contact with the downstream ends of each cylinder. Readout was via a resistor bridge network and a scanning digital voltmeter[5] (DVM) with paper tape printer.

B. Thermal Calibration

Each set of six thermistors was calibrated simultaneously in a constant-temperature forced-draft oven using a National Bureau of Standards-calibrated thermometer[6]. The known systematic errors of this thermometer (approximately 0.03°C) were incorporated into the data analysis. The major uncertainty in the calibration was due to the random error (approximately 0.1°C) in reading the thermometer. The resistance of each thermistor was measured at approximately 20 temperatures between 20 and 80°C. It was parametrized as follows:

$$R_i(T) = R_i(T_o) \exp \{B_i \left(\frac{1}{T} - \frac{1}{T_o}\right)\}$$

where $R_i(T)$ is the resistance of the ith thermistor at the temperature T; and

$$B_i = \frac{X_{1i}}{T} + X_{2i} + X_{3i}T + X_{4i}T^2.$$

This parametrization reproduced the calibration data to about a millivolt, equivalent to about 0.05 degree at 30°C, and about 0.2 degree at 70°C. Although the absolute calibration error increased by a factor of 4 from 30° to 70°, the fractional uncertainty in measuring temperature increments above 30°C remained close to 0.7% for increments between 10 and 40°C.

C. Irradiation

Each set of insulated samples was mounted in a rigid metal frame. An extra frame was used to hold two widely-spaced

fluorescent flags. This frame and two frames containing targets were mounted on a movable table whose height and position transverse to the beam could be remotely controlled.

Prior to irradiation, the axes of the two targets and the (to within ± 0.5 mm), and parallel to the beam direction. The horizontal spacings between the three target frames was also carefully measured. The entire apparatus was then moved out of the beam until the irradiation began.

At the start of an irradiation, the table was moved horizontally and vertically until the beam was centered on both scintillator flags, as observed on closed circuit TV. Then the accelerator was turned off while the table was moved horizontally to place a target assembly in the beam line. The accelerator was turned back on until the desired number of protons, as monitored on a Secondary Emission Monitor (SEM), hit the target. The incident number of protons was chosen to give maximum temperature rises between 20°C and 40°C. This number ranged from 6.7×10^{11} protons for W to 8.8×10^{13} protons for Be.

The beam had a nominal energy of 300 GeV, and was horizontally converging at 1 mrad at our target location. The cross section and position of the beam was obtained by the discoloration of radiosensitive detectors[7] and by autoradiographs of thin activation foils. The approximate average cross section so determined was 2 mm x 8 mm; this was used as input to the Monte Carlo calculations described below.

Temperature readings were taken at the rate of one segment per second, beginning several minutes before the start of the

irradiation. They usually continued for five or more minutes after the irradiation. Typical raw data are shown in Fig. 2.

The number of incident protons was always monitored by a SEM upstream of our target assembly. Because of drifts which were discovered in this device, it was calibrated by radiochemical techniques before and after some of the later runs. The corrections necessary to compensate for the SEM drift are discussed below.

III. DATA ANALYSIS

A. Idealized Situation

In this initial discussion a number of transient effects and the variation of the specific heat, C_p, with temperature are ignored. The temperature T, of each target segment above the ambient temperature T_o is given by:

$$\frac{dT}{dt} = bI - a(T - T_o)$$

where I is the constant incident proton current, a and b are appropriate constants, and heat losses are taken to be proportional to the temperature difference with the ambient. During irradiation:

$$\Delta T(t) \equiv T(t) - T_o = \frac{b}{a} I \ (1 - e^{-at});$$

where t is the time elapsed since the start of the irradiation. Following an irradiation time t_i and a cooling time t'

$$\Delta T(t) = \left[\frac{b}{a} I(1 - e^{-at_i})\right] e^{-at'}$$

where $t = t_i + t'$.

The cooling constant, a, and the temperature at the end of the irradiation, $T_i = T(t_i)$ may be obtained from a least squares fit to the cooling curve of the sample.

We may then correct for the heat lost during irradiation to obtain the adiabatic temperature rise, $\Delta T_c = bIt_i$. This is proportional to the total energy deposited in the sample. Dividing ΔT_c by the number of incident protons, It_i, gives the corrected temperature rise per incident proton, b.

B. Actual Data Analysis

The raw data consisted of a series of DVM readings, taken six seconds apart, for each segment. These readings were first converted to their equivalent temperatures. Several thermal effects must be considered: The finite heat conductivity of the target materials, heat losses into the foam insulation, and heat leaks between target segments.

The short-term behavior of representative samples may be seen in Fig. 2. The apparent cooling or heating of some samples just after the irradiation is due to the existence of a thermal gradient along some samples after each beam pulse, and to the placement of the thermistors in the downstream ends of the target bars. For example, if the bar is upstream of the cascade maximum, then its downstream end is initially warmer than its upstream end, causing the downstream end to cool as the bar approaches thermal equilibrium. The magnitude of this effect was at most 10% of the total temperature rise, and usually less. From the theory of heat conduction one can calculate the thermal relaxation time constant of each segment. For the longest (λ) W and Be bars, these times

are 15 and 200 seconds, respectively. Time constants for equivalent length samples of the other materials lie between these values; for shorter samples the relaxation times are smaller.

During the thermal stabilization, heat loss occurs, and the stabilized samples measured temperature is no longer equal to its average temperature at the end of the irradiation. Heat transfer between adjacent segments was negligible.

All of these effects were handled as outlined in III A above. An exponential cooling curve was fit to those temperatures measured after each target cylinder had reached internal thermal equilibrium. The cooling time constants determined from the least squares fit agreed, to within 10%, with those derived from a simplified thermal model and from separate measurements of the thermal conductivity of the foam insulation. The experimentally determined cooling curve was then extrapolated back to yield the average sample temperature at the end of the irradiation. (Use of non-overlapping portions of the cooling curves generally made less than a 1% difference in the value of the extrapolated temperature rise.) Correcting for heat lost during irradiation then yielded the adiabatic temperature rise. The average specific heat of each element over the observed temperature range was then used to determine the energy deposition in each target cylinder.

Repeated exposures were made for all of the target assemblies. In the early irradiations, a radiochemical calibration of the SEM was not included in each run, but it was later discovered that this SEM drifted about 10% between irradiations. In later runs, the SEM was calibrated using the $Cu(p,x)^{24}Na$ reaction, and an assumed activation cross section of 3.9 mb[7].

The internal consistency and reproducibility of our temperature rise measurements were better than the long-term stability of the SEM, as evidenced by the run-to-run constancy of the ratio of the temperature rises of any two segments of the same sample. This was used as the basis of a two-step normalization process for the 2.54 cm diameter targets to regain the precision of the original thermal measurements. First, we analyzed the irradiations of those targets (Cu, W) which were accompanied by a SEM calibration. These are considered to have an absolute normalization.

The irradiations remaining of the two target assemblies (Al, Be) were not accompanied by a radiochemical SEM calibration. However, each of these targets was irradiated just before or after one of the targets (Cu, W) which did have an absolute normalization made at some other time. We therefore used the average thermal heating of the Cu or W targets as a post hoc SEM calibration for those runs when a radiochemical calibration was lacking. The SEM, assumed to be stable for short periods, was then used to determine the number of protons striking the Al or Be target.

This procedure yielded results which were consistent, within our known measurement errors, for the two Be irradiations. In the case of the Al target, this procedure gave results differing by 6% for the two irradiations. The average of the two results was used for the final answer.

The experimental results for the 2.54 cm diameter targets are presented in terms of GeV cm^{-3} $proton^{-1}$ and $\Delta T/10^{12}$ protons in Fig. 4 a-d. The known measurement errors are smaller than the symbols plotted. All experimental points are subject to a common 8%

additional uncertainty, not included in the stated error, due to the uncertainty in the cross section[9] used for normalization.

It was not possible to use this normalization procedure with the 5.08 cm diameter targets. The uncorrected SEM readings are therefore used as a measure of the incident beam current. Each of these results (Fig. 5a, b) is therefore subject to a normalization uncertainty of 10 - 20%.

IV. MONTE CARLO CALCULATIONS

The Monte Carlo program CASIM was used to calculate the energy deposition in the target assemblies. This program simulates the three-dimensional development of hadron cascades and hadron-initiated electromagnetic cascades. It uses the Hagedorn-Ranft prescription for high energy particle production. More details may be found elsewhere[10].

For the present comparison, the exact geometry of each target assembly along with all that was known about beam size and location[11] for each run were included in the calculation. The results of the calculations are also shown in figures 4 and 5. The horizontal bars which represent the calculated results have been linked across the space between segments to improve the clarity of the graph. The statistical errors in the calculated total energy deposition do not exceed 5%, and are usually less. It must be emphasized that the comparisons between measured and calculated results are made between absolute quantities containing no adjustable normalization.

It is of interest to examine the calculated results for the various mechanisms by which energy is deposited in the targets

as a function of depth and target material. A separate tally was kept in CASIM for the following three contributions: (1) ionization and nuclear excitation due to the incident primary particles (2) ionization and nuclear excitation due to all secondary and higher generation hadrons (3) electromagnetic showers initiated by neutral pions. The results for each of these contributions has been plotted separately in figures 4 and 5.

The energy deposition due to primaries shows the expected exponential decline, interrupted by the gaps. The relative values of the energy deposition are approximately equal in all target cylinders occupying the same position. (The lack of exact equality is entirely due to the difference between the collision lengths assumed in the calculations and the unit target lengths.)

Second, according to the particle production model employed in CASIM, the multiplicities and momentum spectra of the energetic secondaries vary little with atomic mass of the target. This behavior has also been observed experimentally[12], at least qualitatively. This accounts for the similarity in the (scaled) depth dependence of the energy deposition due to secondaries observed in all four cases.

Third, the contribution due to neutral pion-initiated electromagnetic showers retains a strong variation in the depth dependence with atomic number. This is, of course, due to the fact that the radiation length ($\propto AZ^{-2}$) and not the collision length ($\propto A^{1/3}$) governs this depth dependence.

Finally, comparison of the large diameter targets with the corresponding small diameter ones of the same material (Al and

Cu) indicates that there is a greater buildup of energy deposition with depth in the larger diameter targets. This is because, as the cascade broadens with increasing depth, the larger diameter target permits greater energy containment.

It may be tempting to subtract the total energy deposited in the small diameter targets from that of the large targets and compare the energy density in the outer annulus with calculation. However the combined uncertainties of experiment and calculation along with differences in beam position and distribution prevent this comparison from being made in a meaningful way.

V. CONCLUSION

The excellent agreement between the measured and predicted energy deposition curves is strong evidence that the various models and approximations used in CASIM are correct in the narrow target regime. We can therefore confidently use the results of such calculations for other, practical geometries such as production targets, collimators and beam dump cores. Experimental tests of, and bench mark measurements for these calculational techniques are being made on a larger scale.

VI. ACKNOWLEDGEMENT

We would like to thank the Fermilab Meson Department, Operations Section, Alignment Group, and Switchyard Group (L. Oleksiuk in particular) for their indulgence and help in arranging these irradiations. The SEM calibrations were performed by S. Baker and J. Baldwin. This work would not have been possible without the enthusiastic support of all of our technicians, most especially J. Larson and D. Voy.

REFERENCES

[1]J. Ranft, Particle Accelerators 3, 77 (1971); T. W. Armstrong et al., Nucl. Sci. Eng., 49, 82 (1973); A. Van Ginneken and M. Awschalom, "High Energy Particle Interactions in Thick Targets. I. Hadron Cascades, Shielding and Energy Deposition", Fermilab, Batavia, Ill. (1974). These papers also refer to similar earlier works.

[2]Previous similar work at lower energies was reported by L. Henny et al., CERN MPS/CO MD/70-14 (1970) and CERN MPS/CO MD/70-21 (1970).

[3]Average thermal conductivity ~ $1.2 \cdot 10^{-4}$ cm^{-2} sec^{-1} deg^{-1}.

[4]Fenwall model UUT43J1.

[5]Hewlett Packard model 3480B, 3485A.

[6]Fisher model 1B3116.

[7]These consisted of filter paper soaked in a saturated aqueous NaCl solution, then dried and wrapped in clear cellophane tape.

[8]R. C. West, Ed, Handbook of Chemistry and Physics, Chemical Rubber Co., Cleveland, Ohio (1969).

[9]Published results indicate a 3.5 mb cross section at 30 GeV, by which energy the cross section should have been leveled off (J. Hudis et al., Phys. Rev. 129, 434 (1963), N. Porile and S. Tanaka, Phys. Rev. 135, B122 (1964)), but other evidence exists for a 4.0 ± 0.3 mb cross section at 30 GeV. (S. Baker, FN-276. In addition, results from S. B. Kaufman et al., (private communication) combine to yield a 3.9 ± 0.3 mb value at 300 GeV.

[10]A. Van Ginneken, "CASIM: Program to Simulate Transport of Hadronic Cascades in Bulk Matter", Fermilab FN-272 (1975).

[11]Beam Size: 2 x 8 mm; For Be, vertical and horizontal displacements of 2.5 and 3 mm were used; for Al, a vertical displacement of 5 mm was used. All other cases had the beam exactly on axis.

[12]W. Busza et al., Phys. Rev. Lett. 34, 836 (1975).

TABLE I

TARGET MATERIALS USED

Element	Density[a] gm/cm^3	Mean Specific Heat[a] at 25°C cal/gm °C	Unit length of target cm	Non-elastic Mean Free path[b], λ		Radiation length[c], X_o		λ/X_o
				gm/cm^2	cm	gm/cm^2	cm	
$_4$Be	1.85	0.436	35.75	85.4	47.8	70.6	38.2	1.21
$_{13}$Al	2.70	0.215	35.75	113.0	41.8	25.5	9.44	4.43
$_{29}$Cu	8.92	0.0922	14.0	141.0	15.8	13.5	1.51	10.5
$_{74}$W	19.3	0.0316	10.0	190.0	9.86	6.5	0.337	29.2

[a] Ref. 8

[b] For nucleons, A. Ashmore et al., Phys. Rev. Lett., 5, 576 (1960).

[c] H. Davies et al., Phys. Rev. 93, 788 (1954).

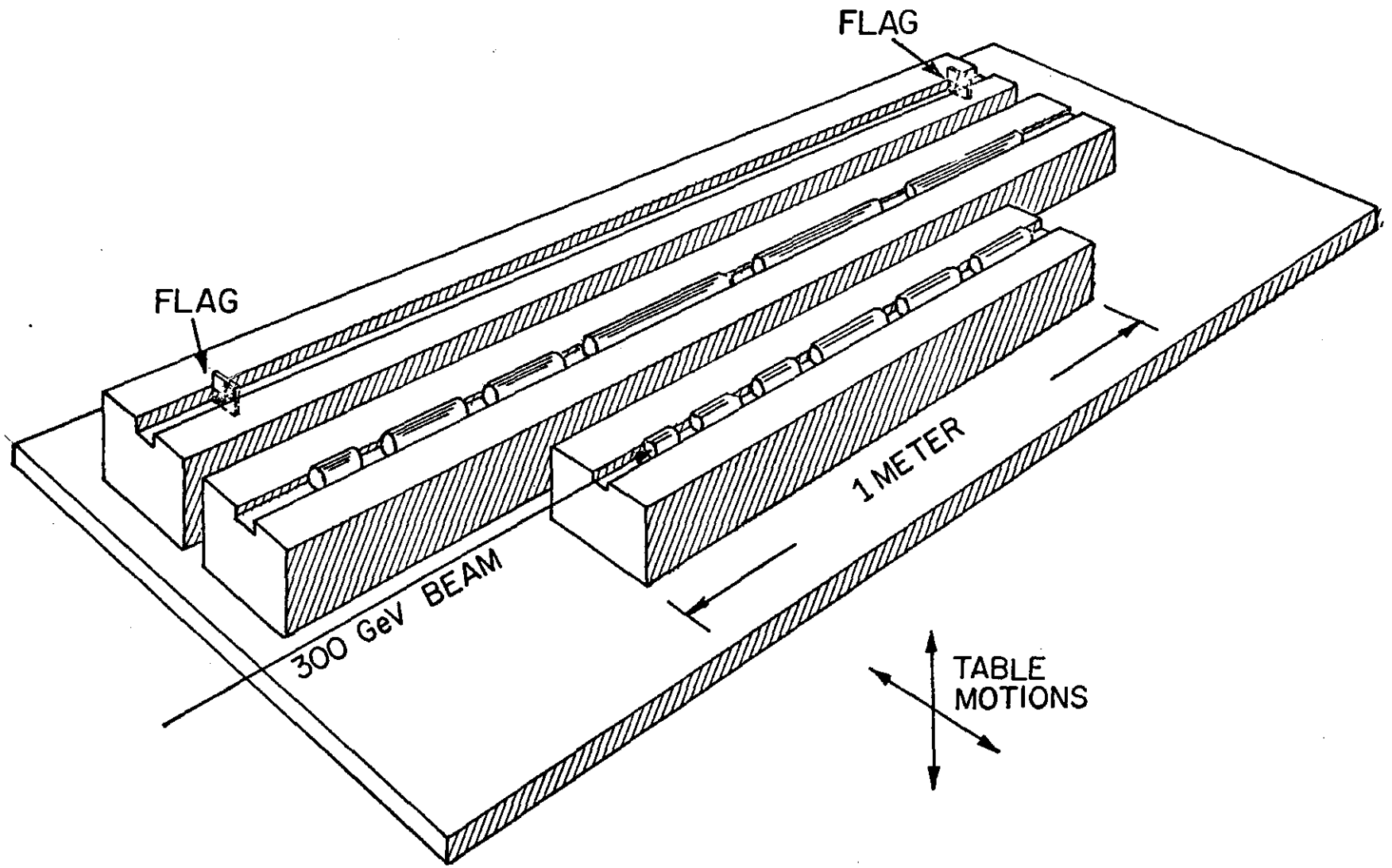

Fig. 1: Apparatus used in target heating measurements, showing placement of scintillator flags, aluminum (center) and copper target assemblies. Thermal insulation between and over target segments is not shown.

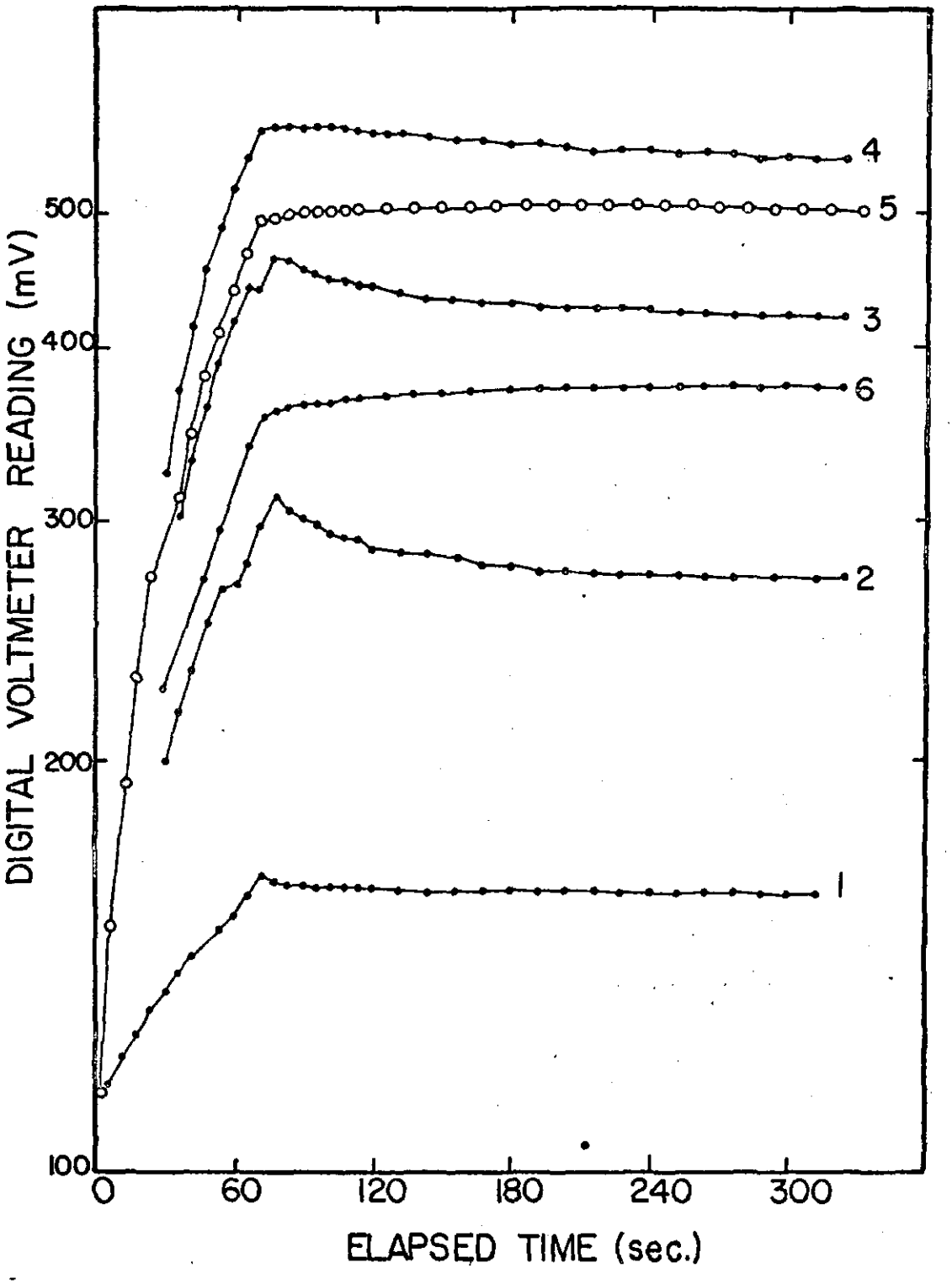

Fig. 2: Typical DVM output data for an irradiation of an aluminum target. The curves are numbered according to the position of the corresponding target segment from the front of the target. Some data are omitted neat t = 0 to improve the clarity of the graph.

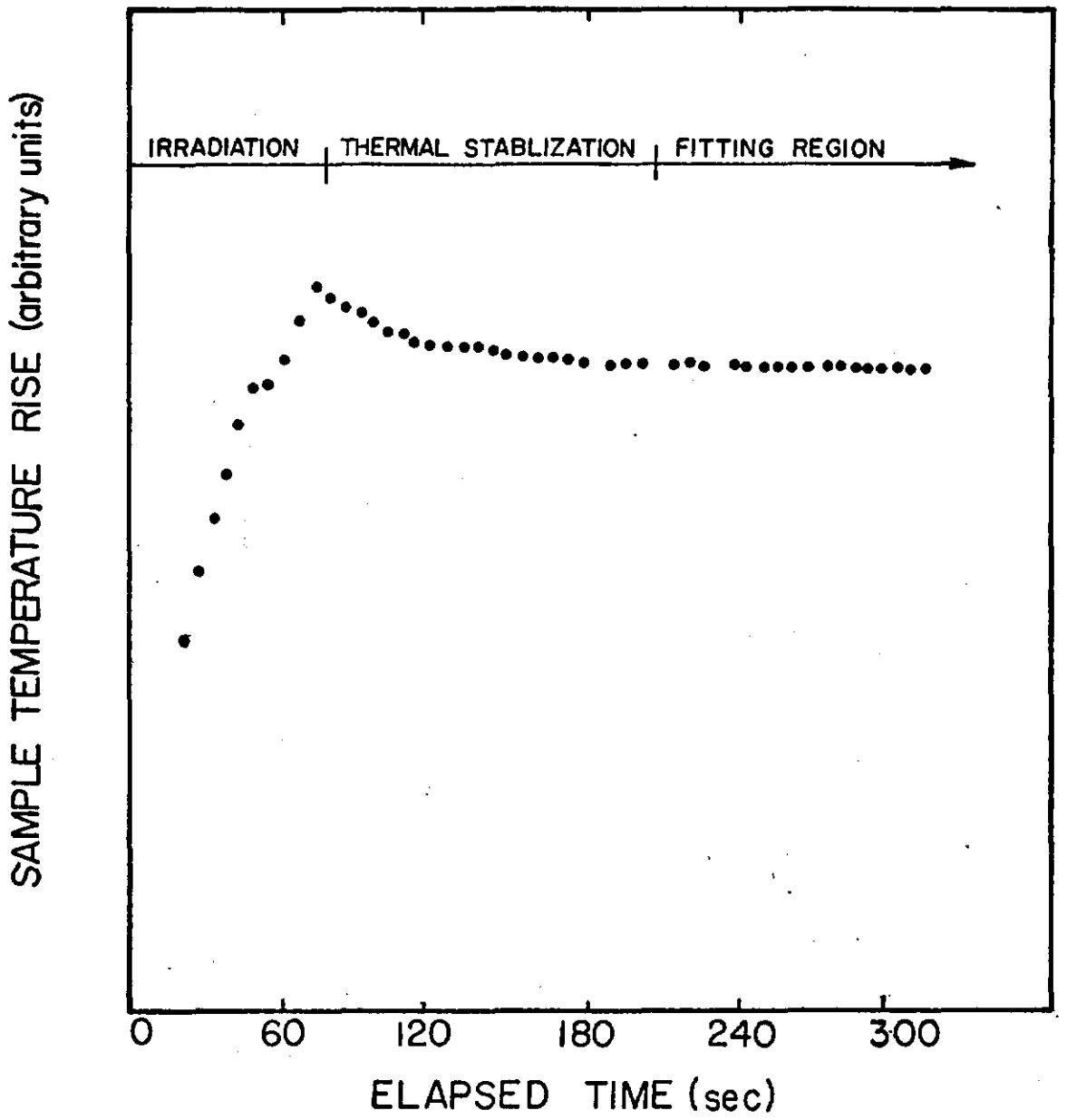

Fig. 3: Schematic representation of the heating of a target segment during irradiation, thermal stabilization just after irradiation, and gradual cooling. Only points in the cooling region were used for a fit to an exponential cooling curve. Compare with typical data in Fig. 2.

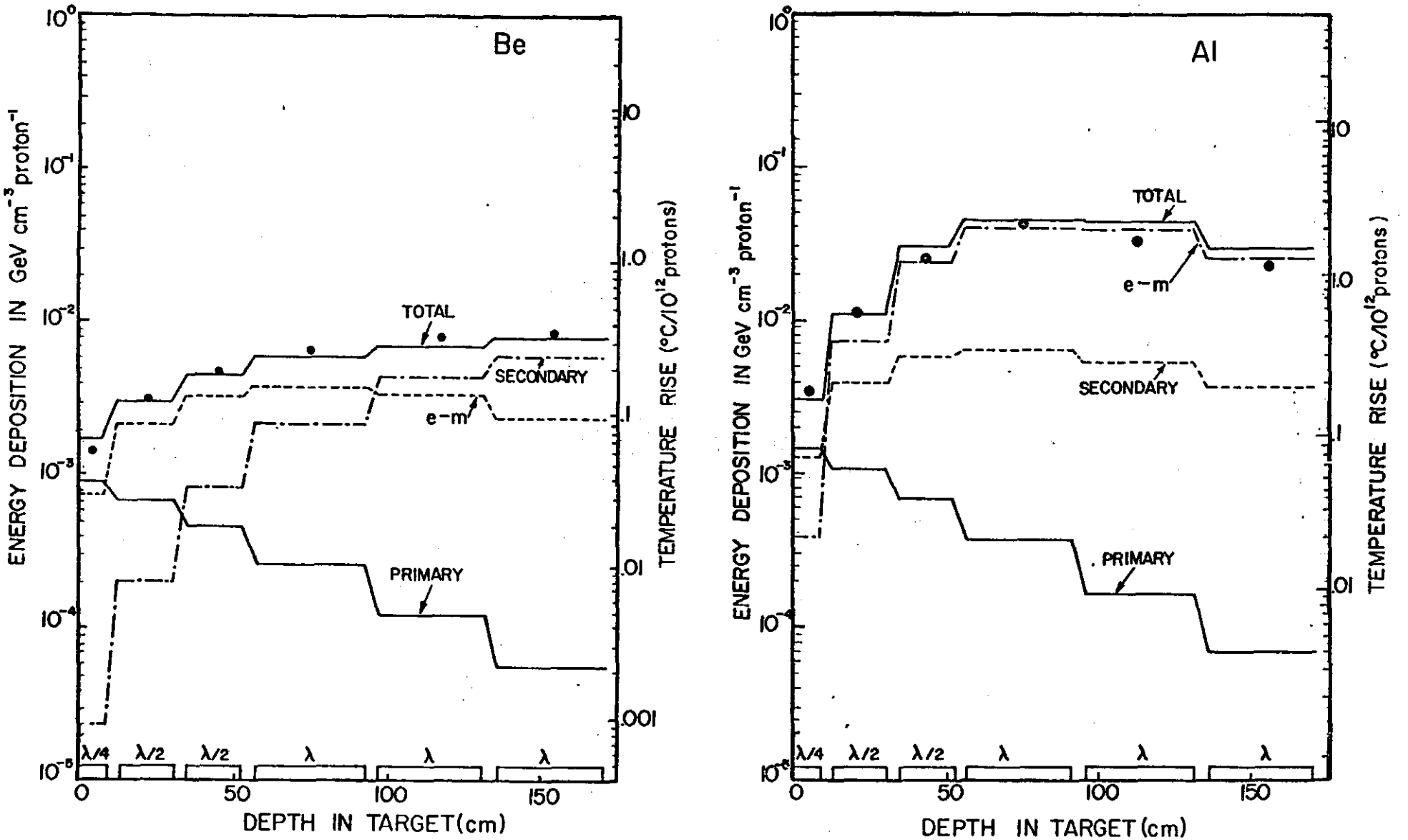

Fig. 4 a, b: Energy deposition as a function of depth for 2.54 cm diameter targets: (a) Be, (b) Al, (c) Cu, (d) W. The target segments are indicated at the bottom of the figure. Points represent measured values. The lines represent calculated total energy deposition, as well as the three components (primary protons, secondaries and electromagnetic showers) comprising the total. The lines representing calculated results have been linked across the spaces between segments for clarity.

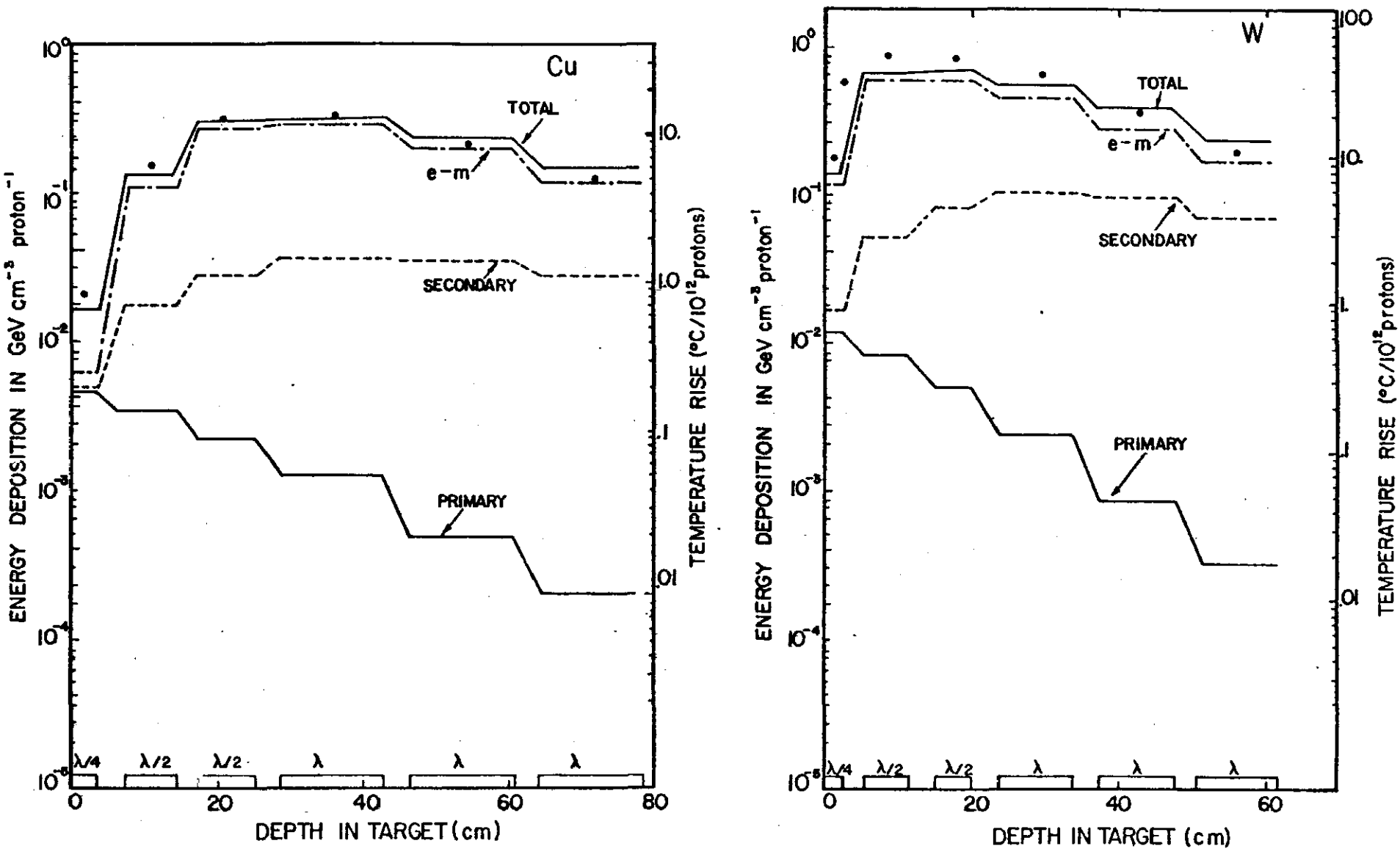

Fig. 4 c, d: Energy deposition as a function of depth for 2.54 cm diameter targets.

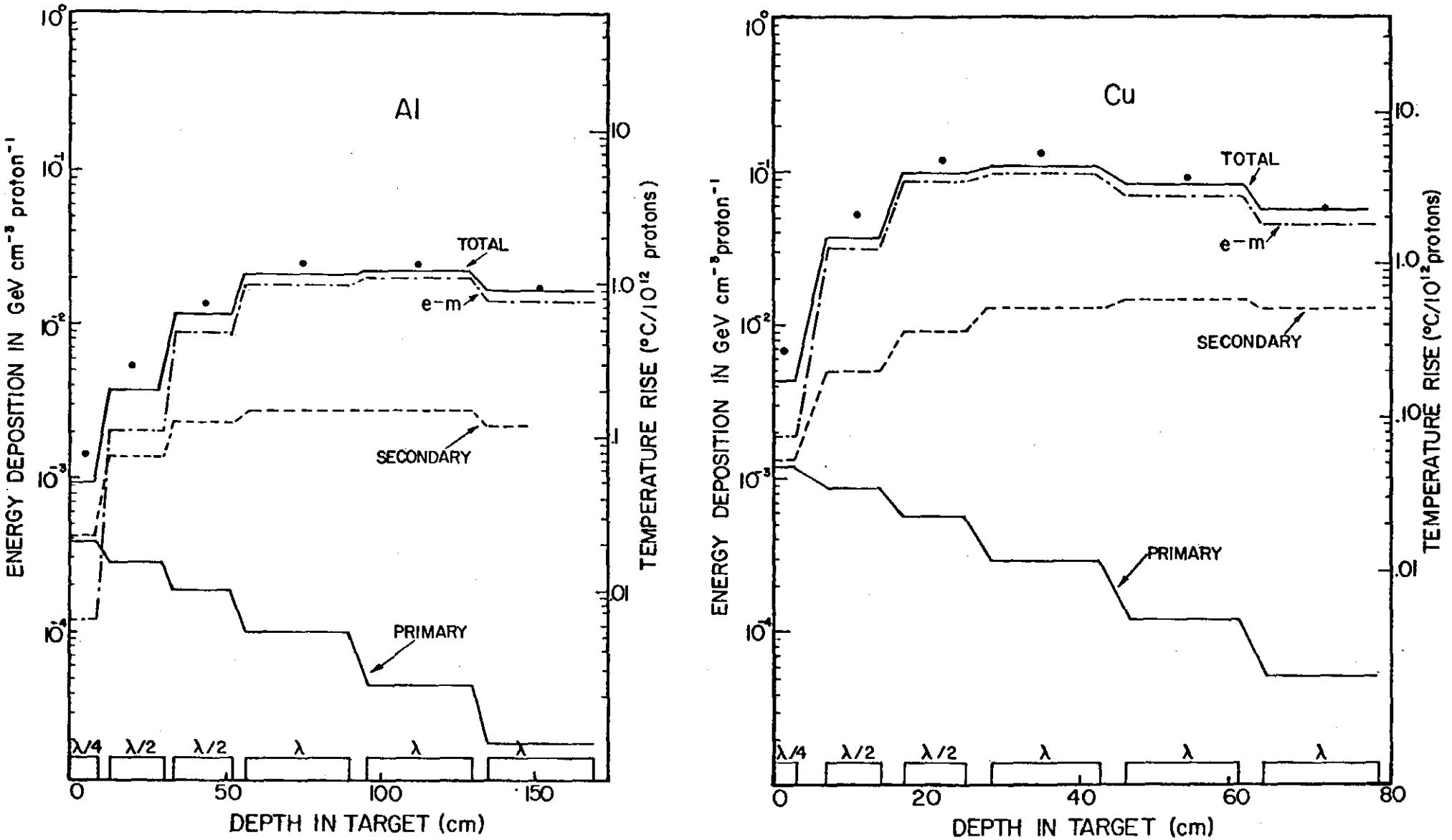

Fig. 5: Energy deposition as a function of depth for 5.08 cm diameter targets: (a) Al, (b) Cu. The same comments apply here as in Fig. 4.